Global Distribution and Morphology of Small Seamounts

Julie Gevorgian[1], David T. Sandwell[1], Yao Yu[1], Seung-Sep Kim[2] and Paul Wessel[3]

[1]Scripps Institution of Oceanography, University of California San Diego, La Jolla, CA, USA
[2]Department of Geological Sciences, Chungnam National University, Daejeon, Korea
[3]Department of Earth Sciences, SOEST, University of Hawaii at Manoa, Honolulu, Hawaii, USA

Corresponding Author: Julie Gevorgian (jgevorgi@ucsd.edu)

Key Points

- We used the latest vertical gravity gradient maps to update and refine a global seamount catalog, finding 10,796 new seamounts.
- Smaller seamounts (< 2500 m tall) having good bathymetry coverage (739) were modeled with a radially symmetric Gaussian function.
- Two modeling approaches show that smaller seamounts have a sigma to height ratio of 2.4 which agrees with an earlier study by Smith (1988).

Abstract

Seamounts are isolated elevations in the seafloor with circular or elliptical plan, comparatively steep slopes, and relatively small summit area (Menard, 1964). The vertical gravity gradient (VGG), which is the curvature of the ocean surface topography derived from satellite altimeter measurements, has been used to map the global distribution of seamounts (Kim & Wessel, 2011). We used the latest grid of VGG to update and refine the global seamount catalog; we identified 10,796 new seamounts, expanding the catalog by 1/3. 739 well-surveyed seamounts, having heights ranging from 421 m to 2500 m, were then used to estimate the typical radially-symmetric seamount morphology. First, an Empirical Orthogonal Function (EOF) analysis was used to demonstrate that these small seamounts have a basal radius that is linearly related to their height – their shapes are scale invariant. Two methods were then used to compute this characteristic base to height ratio: an average Gaussian fit to the stack of all profiles and an individual Gaussian fit for each seamount in the sample. The first method combined the radial normalized height data from all 739 seamounts to form median and median-absolute deviation. These data were fit by a 3-parameter Gaussian model that explained 99.82% of the variance. The second method used the Gaussian function to individually model each seamount in the sample and further establish the Gaussian model. Using this characteristic Gaussian shape we show that VGG can be used to estimate the height of small seamounts to an accuracy of ~270 m.

1 Introduction

1.1 What are Seamounts?

The ocean floor consists of primary tectonic features that form at spreading ridges including abyssal hills, transform faults, and propagating ridges as well as seamounts that form away from the ridges. Seamounts are active or extinct volcanoes with heights that reach at least 1000 meters (Menard, 1964) although this definition has been broadened to include much smaller isolated volcanoes (Staudigel, 2010). Their basaltic composition indicates that they are volcanic in origin and formed in one of three tectonic settings: near mid-ocean ridges, intraplate hotspots, and island arcs (Wessel, 2007). 1) The majority of seamounts form near mid-ocean ridges. The lithosphere at divergent plate boundaries is thin and fractured; this allows magma to propagate through the lithosphere and form small seamounts that are tens to thousands of meters high (Batiza, 1981; Smith & Cann, 1990; Wessel, 2007). 2) Intraplate seamounts that form away from the spreading ridges, usually on older seafloor, are generally attributed to hotspots (Vogt, 1974; Wessel, 2007). The hotspot hypothesis states that as the plate passes over a relatively stationary mantle upwelling (i.e., plume), melt generated at the lithosphere/asthenosphere migrates to the surface forming an age-progressive seamount chain (Wilson, 1963; Morgan, 1971). 3) Island arc seamounts form in the overriding plate at subduction zones. When the oceanic crust of the subducting plate reaches a depth of about 150 km the basalt transforms to eclogite and releases water that lowers the melting temperature in the mantle wedge that erupts, forming island arc volcanoes (Fryer 1996).

The means of formation also has an effect on seamount size and distribution. For one, flanks of spreading centers tend to have many small seamounts (< 3 km tall) since the lithosphere is thin (Batiza, 1981). However, if a seamount is created by a mantle plume beneath thick lithosphere, it can reach a peak of 3 - 10 km above sea level (Wessel, 2007). The distribution of seamounts differs among ocean basins and this variation can be due to the distribution of mantle plumes as well as changes in intraplate stresses. Researchers have found that the global distribution of seamounts height follows an exponential or a power-law model (Smith & Jordan, 1988; Wessel, 1997; 2001). This model suggests that the majority of seamounts are small and there could be 50 to 100 thousand seamounts with heights above 1 km (Wessel, 2007; Kim & Wessel, 2011). Therefore, there is an age to size relationship in seamounts; smaller seamounts generally form on young, thin lithosphere, while larger seamounts generally form on older, thicker lithosphere (Vogt, 1974; Watts et al., 2006).

The global distribution of seamounts is still incomplete because only 20% of the seafloor has been mapped by ships (Mayer et al., 2018). However, seamounts are valuable characteristics of the ocean floor since they provide insight on many of the Earth's geological, oceanographical, and ecological cycles and processes (Wessel, 2007). 1) From a geological perspective, seamounts are particularly important because they are windows into the composition and temperature of the mantle (Koppers & Watts, 2010). Scientists study seamounts to keep track of the changing chemical composition of lava and further understand the eruption process. They can also be used to explain the planet's tectonic evolution since plume-generated seamount chains serve as a record of absolute plate motion (Morgan, 1971; Müller & Seton, 2015). 2) From an oceanographic perspective ocean floor bathymetry has an important effect on ocean circulation: large seafloor features such as ridges and plateaus act as barriers that inhibit deep cold water to mix with the warm water of the ocean surface (Roden et al., 1982). Recent studies suggest that smaller features such as seamounts can also play an important role oceanographically and have a greater influence on circulation which can help scientists better understand the uptake of heat and carbon dioxide in the ocean (Jayne et al., 2004). 3) From an ecological perspective, seamounts are centers for diverse biological communities. The ocean upwelling due to the presence of seamounts brings valuable nutrients from the deep water to the surface. This allows them to become the ideal habitat for fish and a variety of oceanic flora and fauna (Rogers, 1994; Price & Clague, 2002). The impact that seamounts have on the ocean and ecosystems makes them important features to study, map, and classify.

1.2 Mapping Seamounts

There are two main approaches for mapping seamounts – topographic mapping by multibeam sonar on ships and gravity field mapping by satellite altimetry. Multibeam sonar mapping by oceangoing research vessels provides high resolution topography (100-200 m) (Epp & Smoot, 1989) although a great amount of the ocean (~80%) remains unmapped because of the large gap between ship tracks (Mayer et al., 2018). The majority of research surveys have been near mid-ocean ridges for the characterization of small seamounts that formed on the young lithosphere (Wessel et al., 2010). Swath surveys in remote areas or along transit cruises commonly map only the flanks of a seamount so its height is poorly known (Wessel et al., 2010). Complete multibeam coverage of the global seafloor is time-consuming and expensive (Vogt & Jung, 2000) so scientists have turned to satellite altimetry to obtain a low-resolution (~ 6 km) but global mapping.

Previous studies have shown that gravitational anomalies, derived from satellite altimetry, can be used to find larger seamounts (> 2 km tall) (Lazarewicz & Schwank, 1982; Watts & Ribe, 1987; Craig & Sandwell, 1988; Wessel, 1997). Satellite altimeters measure the geoid height which, through Laplace's equation, can be converted to deflections of the vertical, gravity anomalies, or vertical gravity gradient (VGG) (Sandwell & Smith, 2009). There are four main error sources when detecting and mapping seamounts from satellite-derived anomalies: upward continuation, measurement noise, seafloor roughness, and sediment cover (Wessel et al., 2010). (1) Upward continuation causes seamounts with diameters less than the mean ocean depth (~4 km) to be smoothed and attenuated. (2) Ocean waves and currents introduce noise in the satellite altimeter measurements so short wavelength gravity anomalies (< 20 km) are oftentimes not recovered (Garcia et al., 2014). (3) The third issue in detecting seamounts in satellite altimetry is there are a number of features that contribute to small scale gravity anomalies, including abyssal hills and ridges, and their signals can be confused with those of seamounts. (4) Lastly, older small seamounts are oftentimes covered by sediment on the seafloor. The gravity anomaly will still appear above the buried seamount even though it is not visible in the topography (Sandwell et al., 2014).

Detection and mapping of smaller seamounts (< 2 km) has relied on multibeam surveys. In a study conducted by Smith (1988), multibeam (SeaBeam) data of 85 seamounts from the Pacific Ocean were analyzed. She found that there is a relatively uniform base radius to height (*h*) of 0.21 (Figure 1) although there are variations in shape and flatness. Large seamounts in particular tend to be pointier and have smaller flatness values defined by f = d_t/d_b, where d_t is the summit diameter and d_b is the basal diameter (Smith 1988). It was also found that the slope angle, defined by ϕ=arctan(ε) where ε=2h/(d_b- d_t), was equal to ~15 degrees (Smith 1988). As seamount height decreases, the flatness generally increases. Small seamounts are much flatter and have a slope angle proportional to summit height (Smith, 1988).

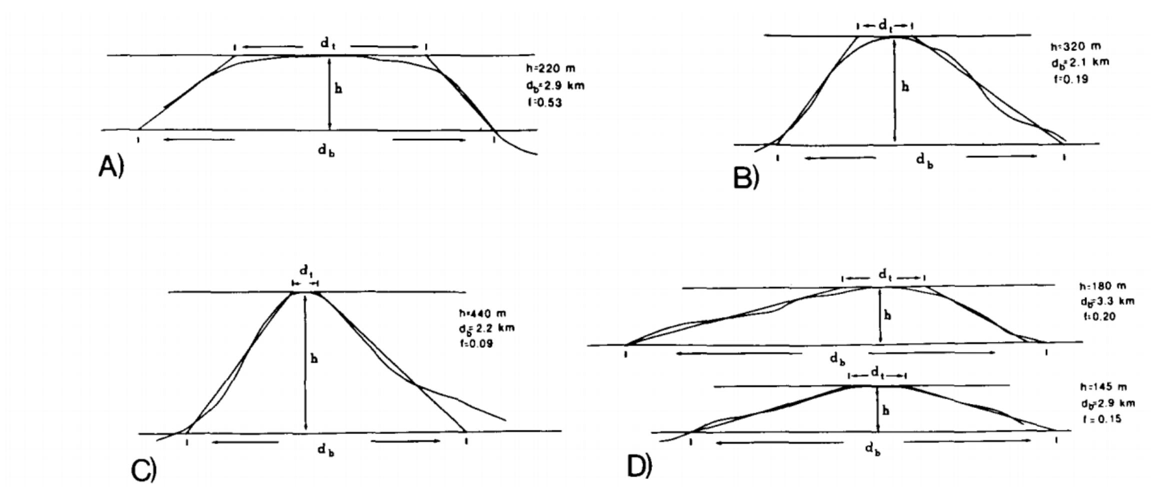

Figure 1. The cross-sectional profiles of four small seamounts (Smith 1988), where *h* is the seamount height, d_b is the basal diameter, *and* d_t *is* the diameter of the flattish summit. Flatness, *f*, is defined by d_t/d_b while the height to basal radius ratio is defined by $2h/d_b$.

1.3 Detecting Seamounts in Satellite Altimetry

Satellite altimetry is a valuable tool for estimating global topography at relatively low spatial resolution (~6 km) and helping scientists find medium to large seamounts. The first global seamount maps were created from Seasat altimeter profiles. Seasat was launched in 1978 and collected sea surface profiles for just 105 days, which resulted in diamond shaped data gaps with dimensions of ~100 km (Marsh & Martin, 1982). The analysis of Seasat altimetry profiles was able to identify 8556 seamounts using Gaussian-shaped modeling (Craig & Sandwell, 1988). They also found that satellite altimetry can be used to determine the along-track locations of seamount centers with an accuracy of better than 10 km, but the cross-track location was more poorly determined due to the wide track spacing. Another measurable characteristic is the diameter of the seamount which is equal to the distance between the peak and trough of the along-track vertical deflection (i.e., sea surface slope) profile. Their study was able to use the locations of the seamounts to draw conclusions on the global distribution of seamounts. They found that the density of seamounts in the Pacific is higher than the Atlantic or Indian oceans and seamounts preferentially occur on the younger side of large fracture zones (Craig & Sandwell, 1988).

Since the Seasat mission there have been a number of altimeter missions that have greatly improved the accuracy and coverage of the gravity field. This has enabled the construction of the VGG which is the spatial derivative of the gravity field (Rummel & Haagmans, 1990). This spatial derivative amplifies short wavelengths and suppresses long wavelengths so it is a valuable tool for locating smaller features on the ocean floor (Kim & Wessel, 2011). However, the spatial derivative also amplifies short wavelength noise which limits seamount detectability. The recently released VGG version has significantly lower noise levels because of new altimeter data from CryoSat-2, Envisat, and Jason-1 missions (Sandwell et al., 2014). After comparing the old and new VGG published in 2015, it was found that the signal to noise ratio (SNR) has increased about 48%, indicating that multiple altimetry sources can improve gravity data and help find unmapped features on the ocean floor. Over the past 5 years there have been additional advances in SNR so many more seamounts are apparent in the VGG.

2 Update to the Kim Wessel Seamount Catalog

To begin the investigation we constructed high resolution VGG images for Google Earth that allowed for a better visualization of seamounts as well as already-digitized tectonic features. The data sets used in Google Earth included the vertical gravity gradient (VGG) (Sandwell et al., 2021), digitized ridges and seesaw-propagators (Matthews et al., 2011; Wessel et al., 2015), global bathymetry and topography through the use of SRTM15+V2.3 (Tozer et al., 2019), and previous seamounts picked by Kim and Wessel (2011). The newly refined VGG (Version 30) revealed many smaller seamounts as well as resolving individual seamounts along ridges, allowing for interesting findings. In order to choose new locations, we divided the Earth into 30 degree longitude by 30 degrees latitude cells which we then examined one at a time. To identify new seamounts, we avoided seafloor features such as fracture zones, transform faults, ridge axes, and see-saw propagators since these can give signals that may look like seamounts in the VGG. Through this method we were able to identify 10,794 new seamounts, expanding the catalog by one third. The new VGG also helped us to find 514 seamounts that were misidentified in the Kim-Wessel catalog of 24,643 (2011). These included any seamount picks that no longer showed a gravity signal in the VGG. After removing these and finalizing the new picks, the updated catalog came to a total of 34,923 seamounts.

The next step was to recenter all of the seamount picks using the generic mapping tool (GMT; Wessel et al., 2019) and Python. To do this, we searched for the maximum VGG in a 5x5 pixel (~ 5 minute) area around the initial seamount pick. Although the location of the maximum in the VGG is oftentimes not the exact geometric center of the seamount, it is a good reference to use for modeling (Figure 2).

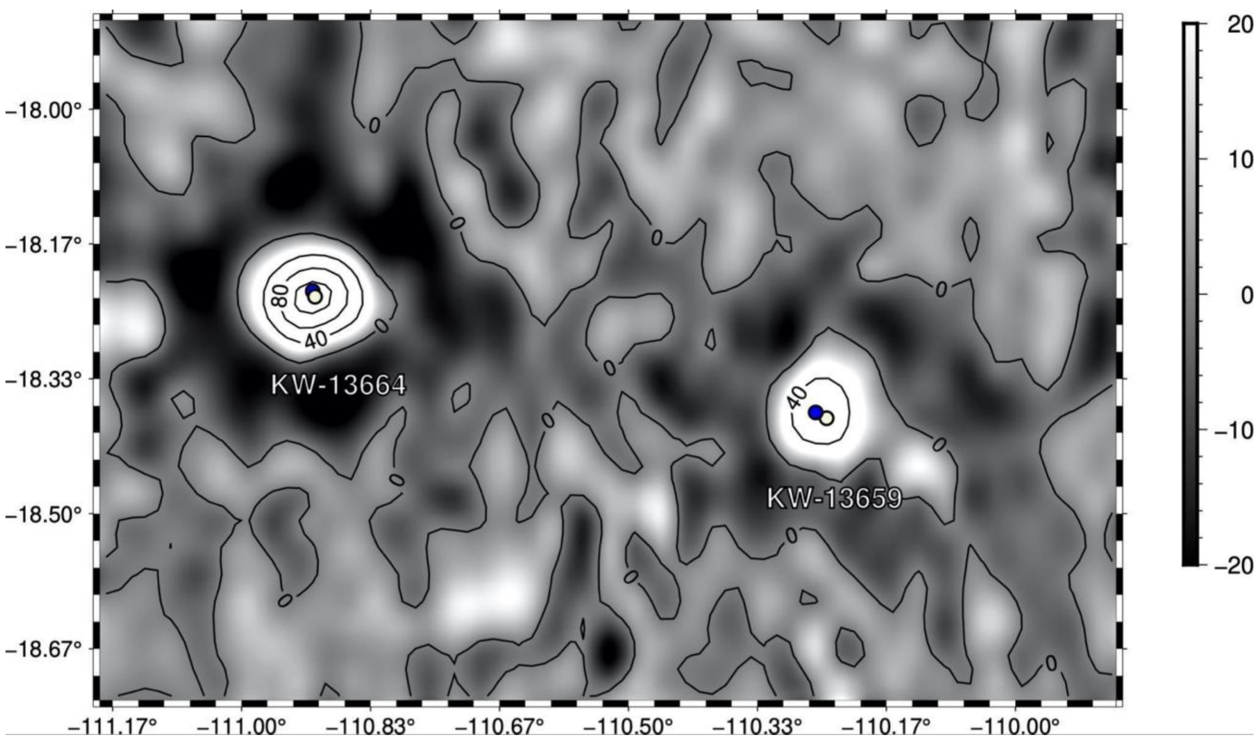

Figure 2. Two seamounts from the Kim-Wessel catalog before and after being centered (20 Eotvos contours). Beige colored points indicate the original location of the seamounts. Dark blue points are the new centers chosen based on the maximum VGG value.

3 Seamount Morphology

3.1 Data Preparation

After the central longitude and latitude were found, we searched the catalog for well-charted seamounts (i.e., those having at least 50% coverage of the seamount and complete coverage of its summit). This search was accomplished by using the source identification grid associated with the SRTM15+V2.3 global bathymetry (Tozer et al., 2019). This process resulted in 739 well charted seamounts < 2500 m tall; 554 from the KW catalog and 185 from the new catalog. An example of a seamount with good data coverage is shown in Figure 3.

For each well-mapped seamount, we calculated the base depth and maximum seamount height. The base depth was taken as the median depth on a 30 km by 30 km area surrounding the center of the seamount. Seamounts are surrounded by relatively flat seafloor so this base depth is well defined by the median of the depth histogram (Figure 3c). The maximum seamount height above the base depth was derived from the shallowest depth in the same area (i.e. summit depth - base depth) (Figure 3d). It is important to note that the maximum seamount height is the shallowest point on the seamount and not necessarily the height at the VGG centered location.

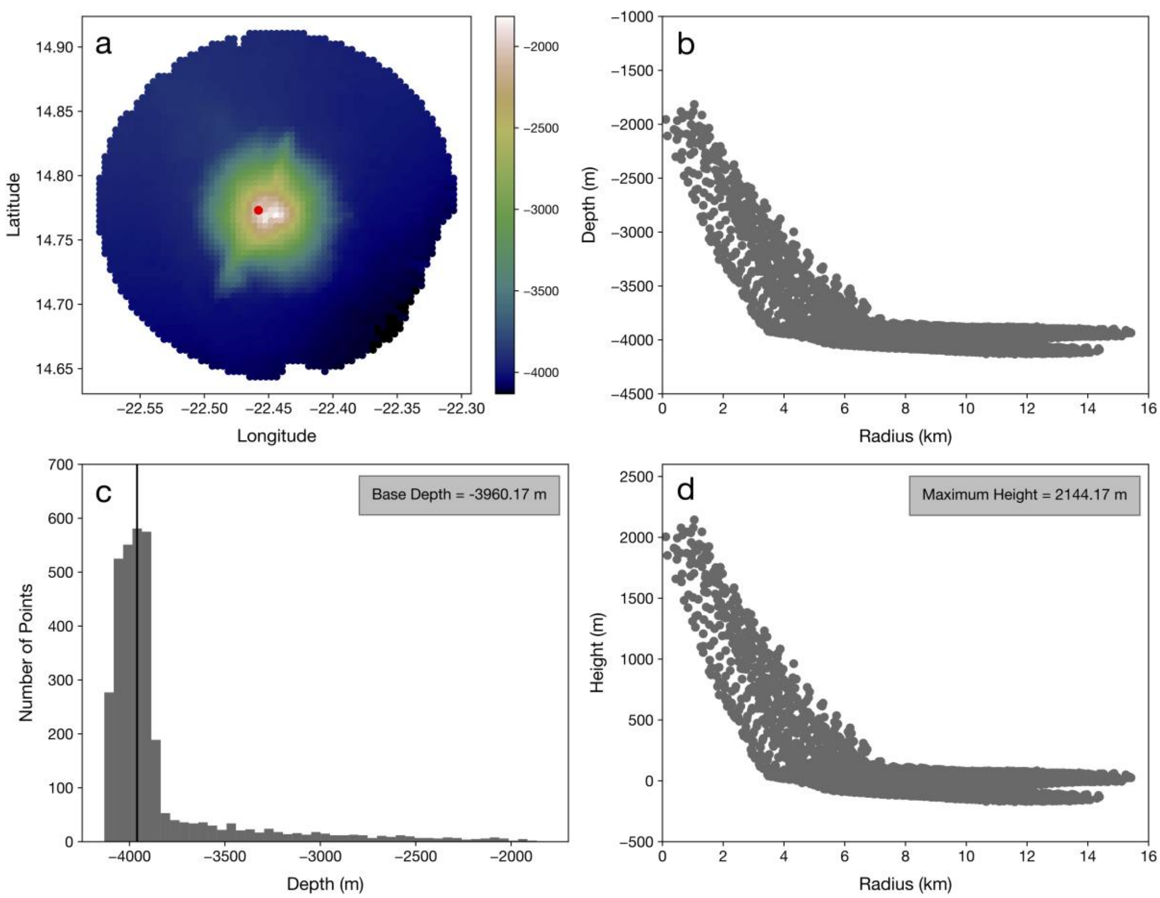

Figure 3. (a) and (b) Seamount KW-00648 depth data within a 15 km radius. The red dot indicates the VGG center of the seamount. (c) A histogram is used to find the base depth. (d) The heights of the data points shifted by base depth.

We use the Empirical Orthogonal Function (EOF) analysis (Hannachi et al., 2007; Preisendorfer & Mobley, 1988) to seek the basic structure of the 739 well charted seamounts. For each seamount, we divide the height and the radius by the maximum height to get the normalized height and normalized radius. We sample the seamounts at fixed normalized radii (0 to 12.5 at 0.5 spacing), and construct a $M \times N$ two-dimensional matrix of the normalized heights at fixed normalized radii, where M is 739 (the number of seamounts) and N is 26 (the number of radius points). The first mode of EOF analysis explains 90.8% of the total variance, thus we neglect all other modes. Its expansion coefficients, which represent the structures in the sampling dimension, resemble a Gaussian shape. Based on this result we assume that each seamount has a radial symmetrical Gaussian shape and a common base to height ratio (i.e. amplitude divided by the standard deviation in Gaussian function). We then use two methods to compute this base to height ratio: an average Gaussian fit to the sample of 739 seamounts and an individual Gaussian fit for each seamount in the sample.

3.2 Method 1: Average Gaussian Fit

To prepare for the average Gaussian fit, the height above the base depth, as well as the radius, for each seamount was normalized by the maximum height. Then the normalized height was median-filtered at 0.5 normalized radius increments using the “filter1d” function in GMT. We then combined the radially normalized height data from all seamounts to obtain the median normalized heights and median absolute deviation. This data was then fit to the following Gaussian equation□

$$y_d = h \cdot e^{\frac{-r^2}{2\sigma^2}} + y_o \quad (1)$$

where r is the seamount normalized radius from 0 to 12.5 with a 0.5 spacing, h is the height, σ is the characteristic width, and y_o is adjusted base depth. This analysis used the median normalized heights for y_d and median-absolute deviation as the error associated to find the h and σ through least square fitting. Since this analysis is done with a profile stack of all the seamounts where the normalized median height converges to zero at larger radii, y_o is set to zero.

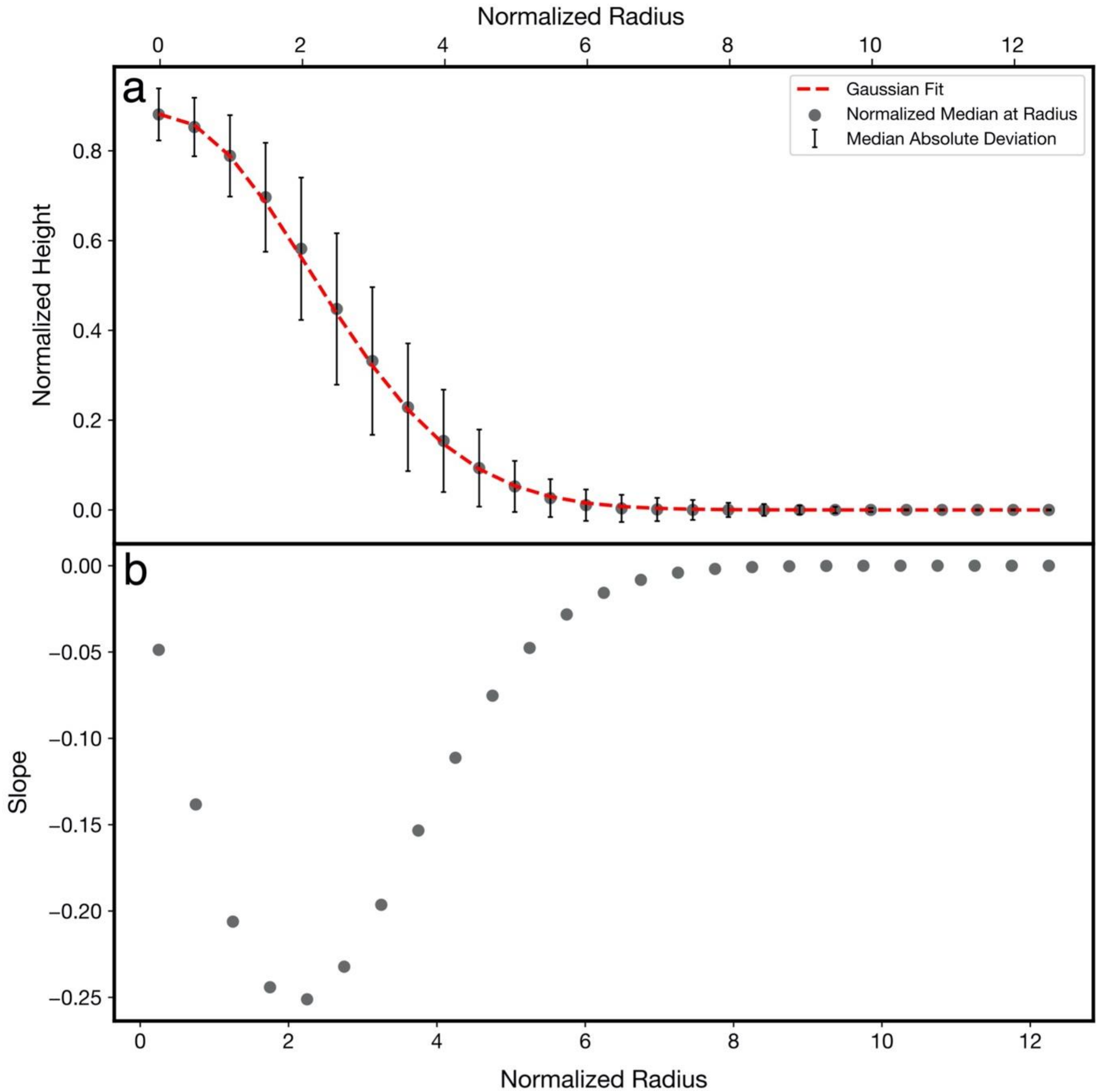

Figure 4. (a) Best fit Gaussian model versus normalized radius has a σ/h= 2.4 (red dashed line); medium value of normalized height (gray dots) and the associated median absolute deviation (gray error bar) versus normalized radius. Note that the normalized height on the y-axis is less than 1 because VGG centering does not always define the maximum height of the seamount as the center. (b) Slope of the Gaussian model has a maximum absolute value of 0.25.

This three-parameter Gaussian model produces the best-fitting height and characteristic width of our collective seamounts (Table 1). Our model had a σ equal to 2.4 h with a maximum absolute slope of 0.25 and explained ~99% of the variance (Figure 4). As discussed below, the maximum absolute slope of the best-fit model is in good agreement with a previous study based on the analysis of 88 seamounts where the seamount height was one fifth of the basal radius (Smith, 1988). The final ratio between sigma and height, σ/h, with a value of ~2.4 is important in defining the final model and ultimately, the gravity field of the Gaussian seamount that is used to construct a new global synthetic bathymetry (SYNBATH) where this factor is used to sharpen the shapes of predicted seamounts (Sandwell et al., 2022).

Table 1. *Gaussian Fit and EOF Analysis Results*

	Number of seamounts	Height h	Sigma σ	$\frac{\sigma}{h}$	Absolute slope	Fraction of variance explained (Gaussian Fit)	Fraction of variance explained (EOF)
Kim-Wessel	554	0.883	2.106	2.385	0.252	~99%	89.9%
New	185	0.849	1.870	2.201	0.272	~99%	90.8%
All	739	0.881	2.112	2.394	0.251	~99%	90.2%

Note. The results from tests run on both the Kim-Wessel seamounts and New seamounts separately in addition to a collective analysis denoted by All.

To evaluate the model, we applied the average Gaussian model to each seamount and computed the difference between topography extracted from the SRTM15+V2.3 and the Gaussian model created using the “grdseamount” function in GMT. GMT “grdseamount” takes the central longitude, central latitude, model height, and radius (3 sigma) as input. We used the median height at the summit of the seamount for the model height. This value is determined by filtering the real data in 0.5 km median increments and finding the maximum. Using the median height at the summit instead of the maximum height allows for less error in the fitting of the model that might have occurred due to singular sharp peaks at the summit. We examined the model fits to all 739 seamounts but only 6 are plotted below (Figure 5) to illustrate some good fits as well as cases where the fits are poor.

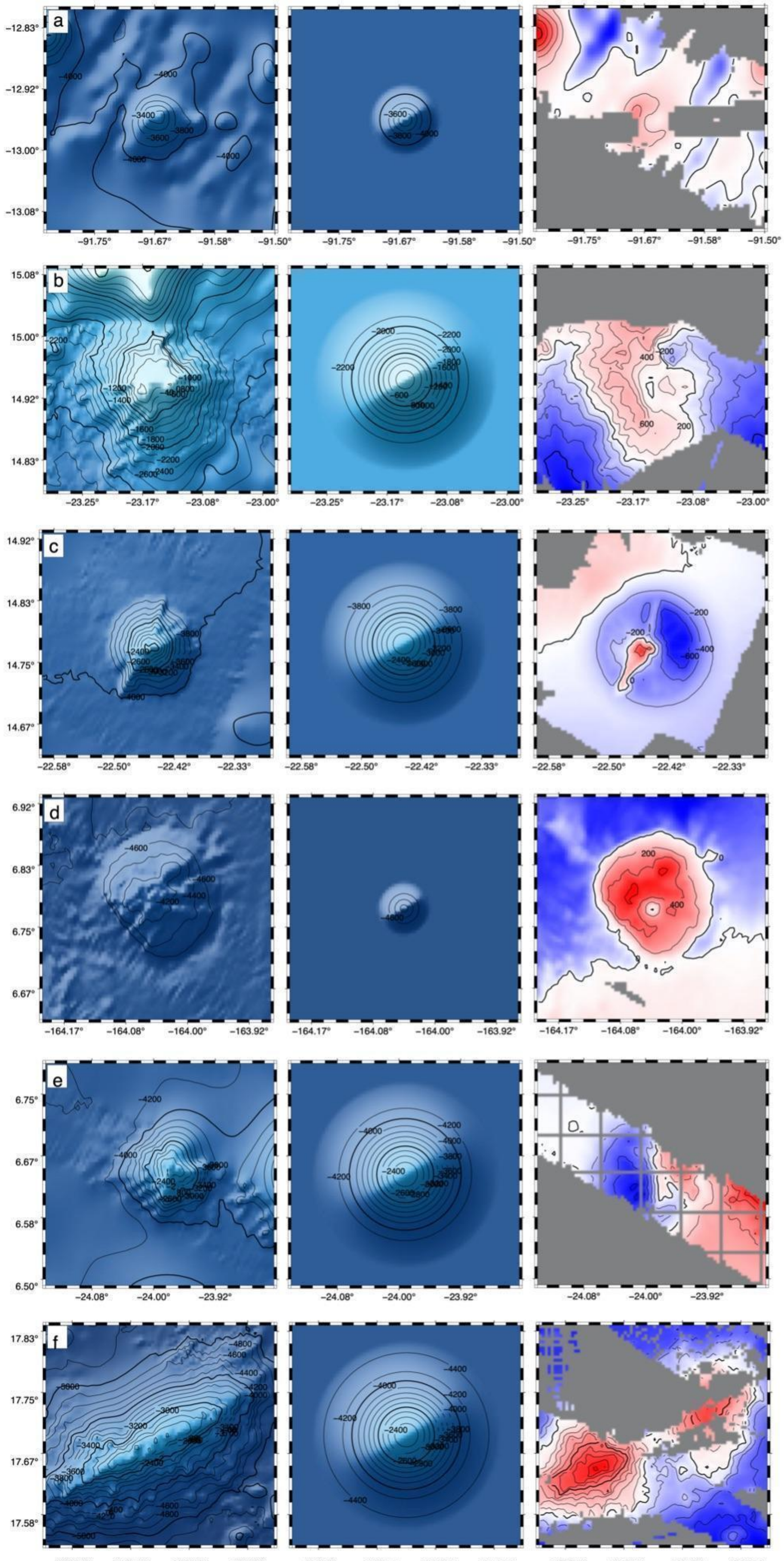

Figure 5. For each seamount example, (left) SRTM15+V2.3 mapped bathymetry, (center) the average Gaussian Model where sigma/h = 2.4, (right) difference between the average Gaussian model and real data. (a) New-08100 is a small seamount with a height of 933 m. The misfit (right) has a scale of ±147 m and a 200 m contour interval. The gray areas have no soundings. (b) KW-00783 shows a good fit for a large seamount with a height of 2099 m. (c) KW-00648 shows an overestimated model fit. In this case the seamount is narrower than the model. (d) KW-15253 shows an underestimated model. In this case the seamount is wider than the model. (e) KW-00543 shows the results from a poorly centered seamount. (f) KW-16423 shows the result of an elliptical seamount that is poorly fitted by a radial Gaussian model.

3.3 Method 2: Individual Gaussian Fit

Since the first method has several seamounts with poor fits, we re-did the analysis by fitting a Gaussian model to each seamount individually. To test which set of seamount height series data is best for this fitting, we compared three types of data: all available bathymetric data, GMT “filter1d”calculated median heights from radii 0-12.5km, and GMT “filter1d” calculated robust median heights from radii 0-12.5km. The results showed that the median and robust median had better fits than the model using all available bathymetric data, but produced very similar results. Because of this, we chose to use the robust median height data for the second analysis.

The robust median height data y_d and radius r input data (unit of km) are fit to equation 1. Each seamount then receives its own unique h , σ , and y_0 values, which are height, sigma, and adjusted base depth respectively. In Figure 6 we have presented the same 6 seamounts as before but with their individual Gaussian fitting.

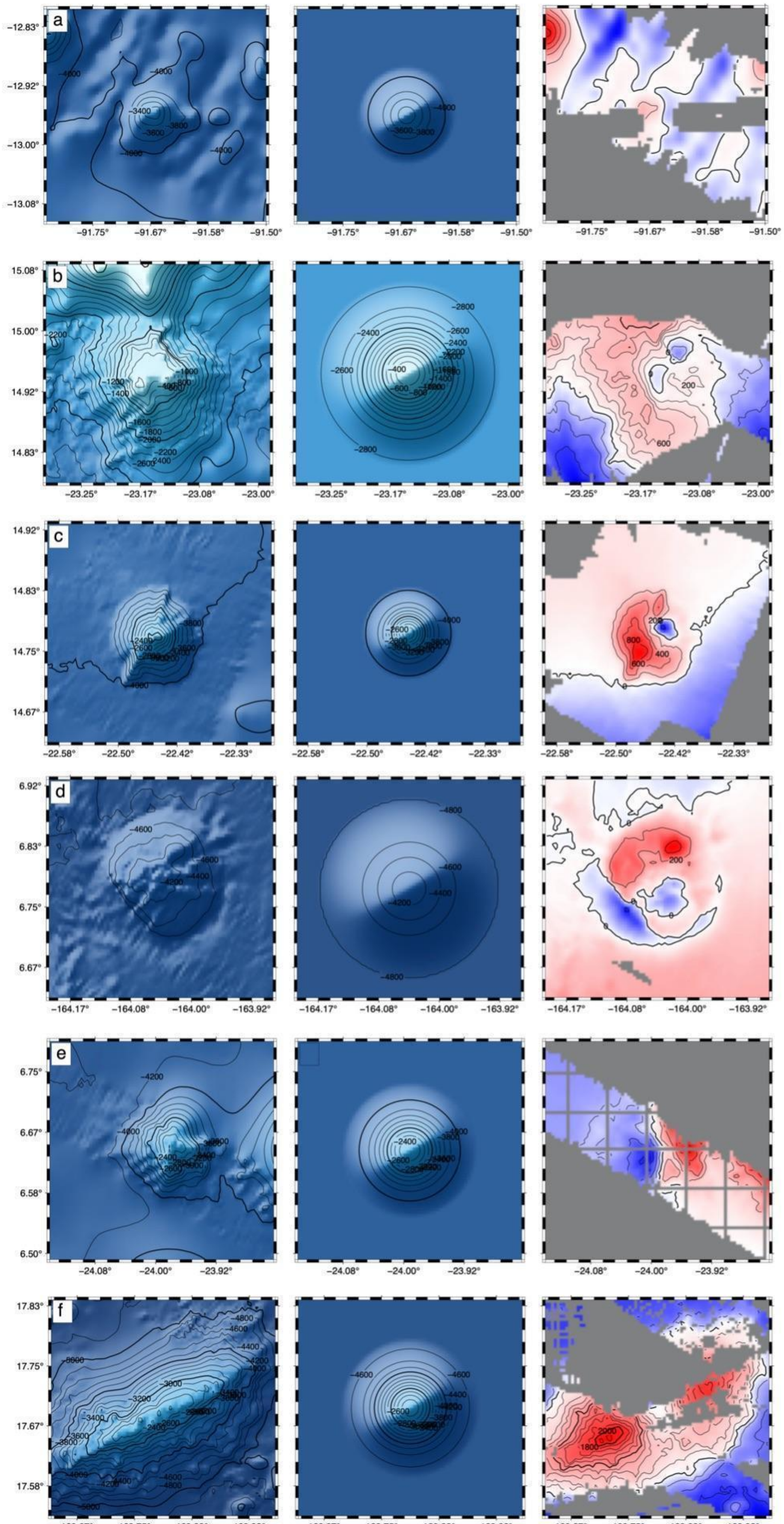
a
−12.83°
−12.92°
−13.00°
−13.08°
−91.75° −91.67° −91.58° −91.50°
b
15.08°
15.00°
14.92°
14.83°
−23.25° −23.17° −23.08° −23.00°
c
14.92°
14.83°
14.75°
14.67°
−22.58° −22.50° −22.42° −22.33°
d
6.92°
6.83°
6.75°
6.67°
−164.17° −164.08° −164.00° −163.92°
e
6.75°
6.67°
6.58°
6.50°
−24.08° −24.00° −23.92°
f
17.83°
17.75°
17.67°
17.58°
169.67° 169.75° 169.83° 169.92°

Figure 6. For each seamount example, (left) SRTM15+V2.3 mapped bathymetry, (center) the individual Gaussian model where sigma/h = 2.4, (right) difference between the individual Gaussian model and real data. a) New-08100. b) KW-00783. c) KW-00648. d) KW-15253. e) KW-00543. f) KW-16423.

The median of the σ/h ratio for these 739 individually fitted seamounts had a value of 2.39 and a mean of 2.6 (Figure 7). This matches well with the value we obtained from the first approach. This indicates that the average seamount fitting and ratio of ~2.4 is a good representation of the morphology of the majority of seamounts.

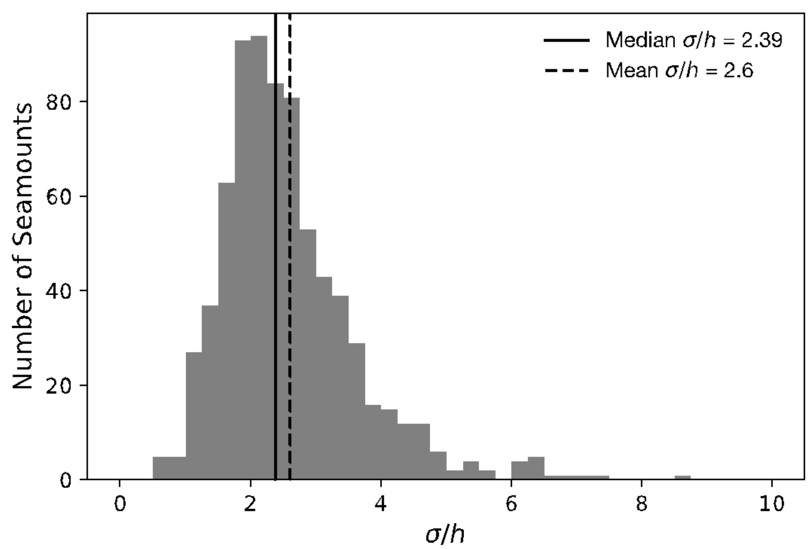

Figure 7. σ/h ratio for the 739 seamounts plotted as a histogram. The median value is 2.39 and mean is 2.6.

4 Discussion

4.1 Comparing Method 1 and Method 2

The relationships between maximum height and model height from Method 1 and Method 2 respectively have been plotted below. Figure 8a shows that the relation between the maximum and model height is linear and therefore, the model serves as a good representation of the seamount height used for the Gaussian analysis. The model height is always less than or equal to the maximum height because the data that we used is filtered with GMT "filter1d" from 0-12.5 radii in 0.5 intervals. Each radius would have the median height value. This would naturally decrease the height value from the maximum height. Figure 8b shows the values for h

height obtained through the individual Gaussian fit against the maximum height of the seamount. Although this graph shows more variability in the data, it generally still follows a linear trend.

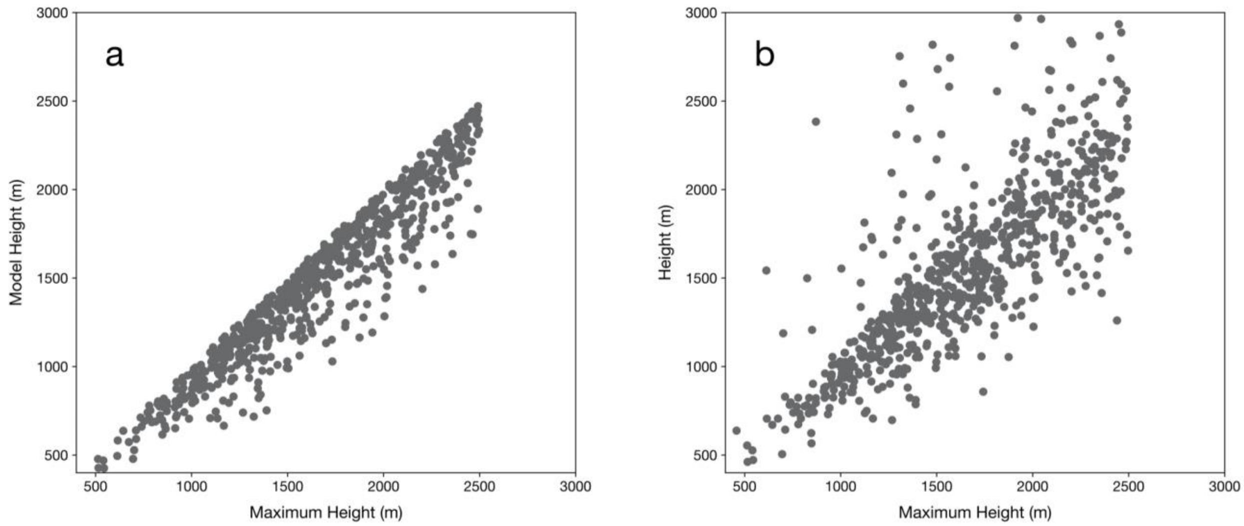

Figure 8. (a) Heights from Method 1 plotted against the maximum heights of the seamounts. (b) Heights Method 2 plotted against the maximum heights of the seamounts.

4.2 Comparing RMS Misfit

The root mean square (RMS) error is calculated from the difference of the model and real topography data available within a 30 by 30 km area. When comparing the results of the average (Fig. 5) and individual (Fig. 6) fitting of these six example seamounts we can see interesting results. From this sample, five of the six seamounts showed a better fit through Method 2. As shown in Table 2 below, we can see that the RMS for all but seamount KW-16423 decreased in error. This is understandable since seamount KW-16423 is elliptical and would not perfectly fit a radially symmetric Gaussian model regardless of the method. For seamounts such as this case, additional parameters such as ellipticity would need to be added for more accurate modeling (Kim & Wessel, 2011).

Table 2. *RMS Misfits for Both Methods*

	Method 1 RMS	Method 2 RMS
New-08100	$\pm$ 147.61 m	$\pm$ 139.75 m

KW-00543	± 340.05 m	± 266.70 m
KW-00648	± 165.63 m	± 160.80 m
KW-00783	± 504.20 m	± 436.32 m
KW-15253	± 158.73 m	± 78.05 m
KW-16423	± 634.81 m	± 698.40 m

Note. The RMS misfits of the six seamounts from Method 1 and 2 calculated from Figure 5c and Figure 6c.

The RMS misfits of all 739 seamounts from both methods are shown in Figure 9. The Average Gaussian fit method shows a slightly wider range in RMS misfit distribution. In contrast, the Individual Gaussian fit method RMS has less variation as the height increases. For both methods however, we see that RMS misfit increases as seamount height increases. This indicates that the height error is typically 20% of the seamount height as shown by the line in Figure 9b.

When comparing the values directly, 472 seamounts showed improvement in the misfit after Method 2 while the other 267 had more error. The RMS of the 472 seamounts improved with a median value of -23.29 m while the RMS of the 267 diminished with a median value of 13.57 m. This shows that Method 2 serves as a better tool for modeling seamounts than Method 1.

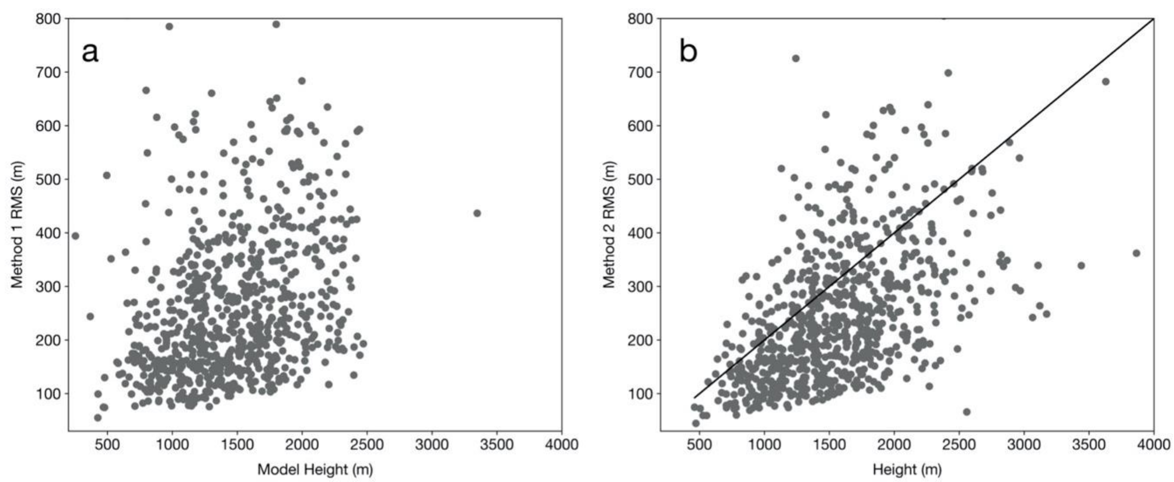

Figure 9. (a) Method 1 Model Heights of seamounts plotted against their RMS. (b) Method 2 heights plotted against each corresponding model RMS.

4.3 Comparing Gaussian Model to Smith (1988)

In Smith (1988), 85 seamounts were analyzed based on their height to base radius ratios. In that study it was found that the seamounts summit height is about one fifth of the basal radius, with a ratio of 0.21. In order to compare the height to base ratio of our own analysis to that of Smith's (who used a flattened cone model as seen in Figure 1 rather than a Gaussian model), we fit a flattened cone model to our average Gaussian model. This allowed us to find that the h/r described by Smith (1988) is approximately the same as h/1.7*σ in our analysis.

Table 3. *Height to Base Ratio Comparison of Smith (1988) and this Study*

85 Seamounts [Smith 1988]	739 Seamounts [this study]
$\frac{h}{r_b} = 0.21$	$\frac{h}{1.7\sigma} = 0.24$

The height to base ratios of the 739 seamounts from our sample and the 85 seamounts described by Smith (1988) are shown in Figure 10.

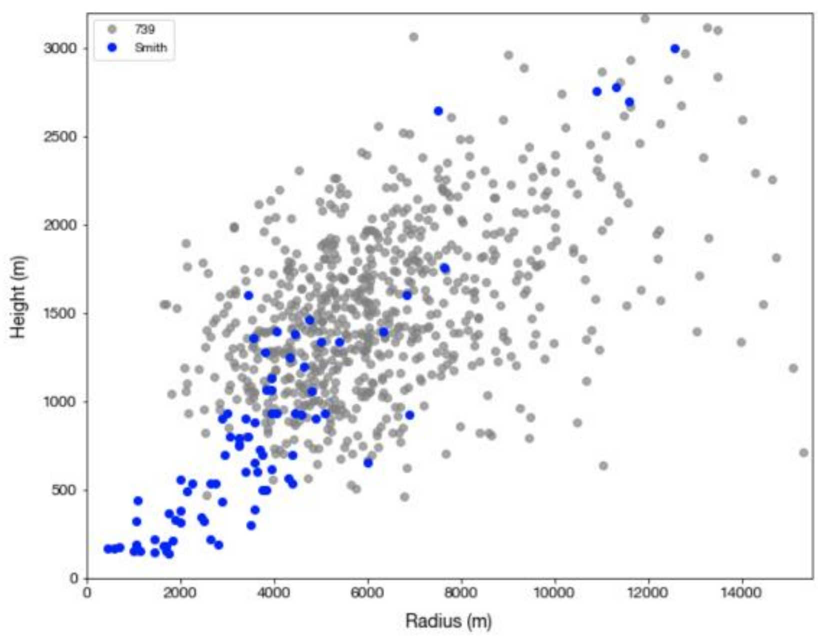

Figure 10. Height vs. base radius of 85 Smith (1988) and our 739 seamounts based on height data from Method 2.

5 Conclusion

Improvement in the vertical gravity gradient allowed us to expand the Kim-Wessel (2011) catalog by 10,794 seamounts. The addition of these new seamounts and refinement of previous picks updated the catalog to a total of 34,923 seamounts. Future improvements in the VGG can further expand our knowledge of seamounts while surveying done by multibeam sonar remains limited.

By modeling a sample of 739 seamounts as a Gaussian we can conclude the following:

1) Two modeling approaches show that medium sized seamounts have a characteristic sigma to height ratio of 2.4 and a maximum slope of 0.25. This is in good agreement with an earlier study by Smith (1988) who found that the summit height is around one fifth of the basal radius.
2) The radially symmetric Gaussian model has significant deviations from actual seamount shape. The way in which the center of the seamount is chosen can also have an effect on the model. It is common that the highest point of the seamount does not correspond to either the largest vertical gravity gradient signal or its geometric center.
3) When comparing the RMS misfit of both Gaussian Model methods, the individual seamount modeling method shows less error. However, both indicate that the error in modeling increases as seamount heights increase.
4) Our Individual Gaussian model was based on three parameters: height, sigma, and basal depth. Including additional parameters such as ellipticity in future analyses can help account for the shape of some seamounts when modeling and provide a better fit.

The modeling of seamounts as a Gaussian can help improve our understanding of their shapes and distribution. Most importantly, the characteristic sigma to height ratio of 2.4 can allow for the modeling of the majority of the seamounts that are identified through satellite altimetry, but have not been surveyed by ships. The VGG and the methods of Gaussian modeling can allow for clarity in understanding the morphology of globally distributed seamounts.

Acknowledgements

This work was supported by the Office of Naval Research (N00014-17-1-2866), NASA SWOT program (NNX16AH64G and 80NSSC20K1138) and the Nippon Foundation through the SeaBed2030 project. S.-S. Kim acknowledges support from the National Research Foundation of Korea (NRF-2021R1A2C1012030). The Generic Mapping Tools (GMT) (Wessel et al., 2019) were extensively used in data processing.

Open Research and Data Availability

Data from our analyses can be found here Seamount_Data and will be uploaded to ZENODO repository. The VGG grids are available in the global_grav_1min folder and the SRTM15+ bathymetry are in the srtm15_plus folder (https://topex.ucsd.edu/pub/). Figures and calculations were performed using GMT (http://www.generic-mapping-tools.org) and Python (https://www.python.org).

References

Batiza, R. (1981). Lithospheric age dependence of off-ridge volcano production in the North Pacific. Geophysical Research Letters, 8(8), 853-856.

Craig, C. & Sandwell, D. T. (1988). Global Distribution of Seamounts from Seasat Profiles. Journal of Geophysical Research, vol. 93, No. B9, p. 10,408-10,420

Epp, D. & Smoot, N. C. (1989). Distribution of seamounts in the North Atlantic. Nature, 337(6204), 254-257.

Fryer, P. (1996). Evolution of the Mariana convergent plate margin system. Reviews of Geophysics, 34, 89–125.

Garcia, E.S., Sandwell, D.T. & Smith, W.H. (2014). Retracking CryoSat-2, Envisat and Jason-1 radar altimetry waveforms for improved gravity field recovery. Geophysical Journal International, 196(3), pp.1402-1422.

Jayne, S.R., St. Laurent, L.C. & Gille, S.T. (2004). Connections between ocean bottom topography and Earth’s climate. Oceanography, 17, 65–74.

Kim, S. & Wessel, P. (2011). New global seamount census from altimetry-derived gravity data. Geophysical Journal International. vol. 186, p. 615-631

Koppers, A. A., & Watts, A. B. (2010). Intraplate seamounts as a window into deep Earth processes. Oceanography, 23(1), 42-57.

Lazarewicz, A. P., & Schwank, D. C. (1982). Detection of uncharted seamounts using satellite altimetry. Geophysical Research Letters, 9(4), 385-388.

Marsh, J. G., & Martin, T. V. (1982). The SEASAT altimeter mean sea surface model. Journal of Geophysical Research: Oceans, 87(C5), 3269-3280.

Matthews, K. J., Muller, R. D., Wessel, P., & Whittaker, J. M. (2011) The tectonic fabric of the ocean basins. Journal of Geophysical Research: Solid Earth, 116(12), 1–28. doi: 10.1029/2011JB008413 https://www.earthbyte.org/category/resources/data-models/tectonic-fabric

Mayer L., Jakobsson, M., Allen, G., Dorschel, B., Falconer, R., Ferrini, V., Lamarche, G., Snaith, H. & Weatherall, P. (2018) The Nippon Foundation—GEBCO seabed 2030 project: The quest to see the world's oceans completely mapped by 2030. Geosciences, 8(2), p.63.

Menard, H. W. (1964) Marine Geology of the Pacific. McGraw Hill, New York

Morgan, W.J. (1971) Convection plumes in the lower mantle. Nature, 230, 43–4.

Müller, R. D. & Seton, M. (2014). Plate Motion. In: Harff J., Meschede M., Petersen S. & Thiede, J. (eds), Encyclopedia of Marine Geosciences. Springer, Dordrecht, pp. 1–10

Price, J.P. & Clague, D.A. (2002). How old is the Hawaiian biota? Geology and phylogeny suggest recent divergence. Proceedings of the Royal Society of London, 269, 2429–35.

Roden, G.I., Taft, B.A. & Ebbesmeyer, C.C. (1982). Oceanographic aspects of the Emperor Seamounts region. Journal of Geophysical Research, 87, 9537–52.

Rogers, A.D. (1994). The biology of seamounts. Advances in Marine Biology, 30, 305–50.

Rummel, R., & Haagmans, R. H. N. (1990). Gravity gradients from satellite altimetry. Marine Geodesy, 14(1), 1-12.

Sandwell, D. T., Goff, J. A., Gevorgian, J., Harper, H., Kim, S., Yao, Y., et al. (2022). Improved Bathymetric Prediction Using Geological Information: SYNBATH. Earth and Space Science, vol. 9, issue 2, doi:10.1029/2021EA002069

Sandwell, D. T., Harper, H., Tozer, B. & Smith, W. H. (2021). Gravity field recovery from geodetic altimeter missions. Advances in Space Research, 68(2), 1059-1072. https://topex.ucsd.edu/pub/global_grav_1min/

Sandwell, D.T., Müller, R.D., Smith, W.H., Garcia, E. & Francis, R. (2014) New global marine gravity model from CryoSat-2 and Jason-1 reveals buried tectonic structure. Science, 346(6205), pp.65-67.

Sandwell, D.T. & Smith, W.H. (2009). Global marine gravity from retracked Geosat and ERS-1 altimetry: Ridge segmentation versus spreading rate. Journal of Geophysical Research: Solid Earth, 114(B1).

Smith, D. (1988). Shape Analysis of Pacific Seamounts. Earth and Planetary Science Letters, vol. 90. p.457-466

Smith, D.K. & Cann, J.R.1 (1990). Hundreds of small volcanoes on the median valley floor of the Mid-Atlantic Ridge at 24–30 N. Nature, 348, 152–5.

Smith, D. & Jordan, T. (1988). Seamount Statistics in the Pacific Ocean. Journal of Geophysical Research, vol. 94, No. B4, p. 2899-2918

Smith, W.H.F. & Sandwell, D.T. (1997). Global seafloor topography from satellite altimetry and ship depth soundings. Science, 277, 1956–62.

Staudigel, H., Koppers, A., Lavelle, W., Pitcher, T. J., & Shank, T. M. (2010). Defining the Word “Seamount”. Oceanography, vol. 23, No 1, p. 20-21.

Tozer, B., Sandwell, D.T., Smith, W.H., Olson, C., Beale, J.R. & Wessel, P. (2019). Global bathymetry and topography at 15 arc sec: SRTM15+. Earth and Space Science, 6(10), pp.1847-1864. https://topex.ucsd.edu/pub/srtm15_plus/

Vogt, P. R. (1974). Volcano spacing, fractures, and thickness of the lithosphere. Earth and Planetary Science Letters, 21(3), 235-252.

Vogt, P. R. & Jung, W.-Y. (2000). GOMaP: A matchless resolution to start the new millennium, Eos Trans. AGU, 81(23), 254– 258, doi:10.1029/00EO00180.

Watts, A. B., Sandwell, D. T., Smith, W. H. F., & Wessel, P. (2006). Global gravity, bathymetry, and the distribution of submarine volcanism through space and time, J. Geophys. Res., 111, B08408, doi:10.1029/2005JB004083.

Watts, A.B. & Ribe, N.M. (1984). On geoid heights and flexure of the lithosphere, J. Geophys. Res., 89, 11,152-11,170

Wessel, P. (1997). Sizes and Ages of Seamounts Using Remote Sensing: Implications for Intraplate Volcanism. Science, vol. 277, p. 802-805

Wessel, P. (2001). Global distribution of seamounts inferred from gridded Geosat/ERS-1 altimetry. Journal of Geophysical Research: Solid Earth, 106(B9), pp.19431-19441.

Wessel, P. (2007). Seamount Characteristics. In: Pitcher T, Morato T, et al., editors. *Seamounts: Ecology, Fisheries, & Conservation.* Fish and Aquatic Resources Series 12. Blackwell Publishing., p. 3-20.

Wessel, P. & Kim, S. (2015). Finding Seamounts with Altimetry-Derived Gravity Data. National Research Foundation.

Wessel, P., Luis, J. F., Uieda, L., Scharroo, R., Wobbe, F., Smith, W. H. F., & Tian, D. (2019). The generic mapping tools version 6. Geochemistry, Geophysics, Geosystems, 20(11), 5556-5564.

Wessel, P., Sandwell, D. T., & Kim, S. (2010). The Global Seamount Census. Special Issue on Mountains in the Sea, Oceanography, vol. 23, No. 1, p. 24-33

Wilson, J.T. (1963). A possible origin of the Hawaiian islands. Canadian Journal of Physics, 41, 863–70.